Membrane potential of single asymmetric nanopores: divalent cations and salt mixtures

Patricio Ramirez,[1,*] Javier Cervera,[2] Vicente Gomez,[1] Mubarak Ali,[3,4] Saima Nasir,[4] Wolfgang Ensinger,[4] and Salvador Mafe[2]

[1]*Departament de Física Aplicada, Universitat Politécnica de València, E-46022 València (Spain)*

[2]*Departament de Física de la Terra i Termodinàmica, Universitat de València, E-46100 Burjassot (Spain)*

[3]*Materials Research Department, GSI Helmholtzzentrum für Schwerionenforschung, D-64291 Darmstadt (Germany)*

[4]*Department of Material- and Geo-Sciences, Technische Universität Darmstadt, D-64287 Darmstadt (Germany)*

ABSTRACT

We study the electric potential difference (*membrane potential*) that arises across a single-pore membrane which separates two aqueous solutions at different salt concentrations. This potential difference is obtained here as the *reversal potential* of a conical nanopore, defined as the applied voltage needed to obtain a zero current through the membrane. To this end, different monovalent (LiCl, NaCl, KCl, and CsCl) and divalent ($CaCl_2$, $MgCl_2$, and $BaCl_2$) salt cations are considered over a wide range of concentrations and salt mixtures for the two asymmetric nanostructure directionalities. The experimental data allows discussing fundamental questions on the interaction of the charges fixed to the pore surface with the mobile ions in solution over nanoscale volumes. In particular, we describe the effects due to (*i*) the relative orientation of the axial charge distribution along the pore and the externally imposed concentration gradient, (*ii*) the different screening of the pore negative charges by the monovalent and divalent cations, and (*iii*) the non-zero bi-ionic potential arising between two salts of distinct cations with a common anion at the same concentration. We have also given a quantitative description of the experimental data obtained with monovalent cations on the basis of the Poisson-Nernst-Planck formalism. In the case of the divalent cations, however, we could give only a qualitative description of the observed phenomena. Taken together, the results can contribute to the understanding of electrochemical and bioelectrical membrane processes which are regulated by the interplay between the membrane asymmetry and the ionic concentration and electrical potential gradients.

Keywords:
Conical nanopore
Membrane potential
Divalent cations
Bi-ionic potential

1. Introduction

The electric potential difference arising across a membrane that separates two aqueous solutions at different salt concentrations can be obtained as the *reversal potential*, which is the applied voltage needed to obtain a zero current through the membrane. We study this electrochemical magnitude for the case of a single-pore membrane consisting of a conical nanopore. To this end, we consider different directionalities for the nanostructure asymmetry using a series of mono and divalent salts over a wide range of concentrations.

There is a renewed interest on membrane processes allowing the conversion between the *input* free energy available in the form of a salt concentration gradient and the *ouput* electrical energy obtained as a potential difference. In addition, ionic concentration gradients and electric potential differences are also central to electrochemical energy storage in batteries, supercapacitors, fuel cells, and desalination. In this context, new technologically-oriented proposals involving environmental systems should be complemented with basic experimental studies under controlled laboratory conditions and new theoretical models [1-17].

The membrane potential is not only significant to energy conversion and storage with artificial membranes but is also an important single-cell bioelectrical characteristic for multicellular processes such as embryogenesis and tumorigenesis [18-20]. Indeed, externally induced changes in the micro-environmental ionic concentrations that determine the cell membrane potential can produce serious effects both at the single-cell and multicellular levels [18,20]. In this context, conical nanopores with surface charges can be considered as *biomimetic nanostructures* closing the gap between artificial and biological membranes [21-24]. These nanoscale pores show ionic selectivity properties that mimic those of the ion channel proteins inserted in the cell membrane when biologically relevant ions such as potassium, sodium, calcium, magnesium, and chloride are used [25].

Remarkably, the carboxylic acid groups located on the nanopore surface [21,22] are also present in most moieties asymmetrically distributed through the axis of typical ion channels [24,25]. As in the case of conical nanopores [21,22], it is the inhomogeneous distribution of membrane fixed charges that allows the current rectification and ionic selectivity phenomena central to most cell membrane functions. Note that the basic mechanism that supports these functions, the electric interaction of the fixed surface charges with the mobile ions in solution, is common to both ion channel and nanopores [22,25-28].

While there is a voluminous literature on membrane potentials in protein ion channels and ion-exchange membranes, including both classical references [25,29-31] and recent reviews [32,33], this is not the case of modern artificial nanostructures. We have previously considered the theoretical description of ionic selectivity in nanopores on the basis of current-voltage (*I-V*) curves, salt fluxes, and membrane potentials [22,34]. In particular, we developed a model for the reversal potential in conical nanopores based on the Poisson and Nernst-Planck (PNP) equations [35] and compared the results obtained with a limited set of data concerning KCl aqueous solutions only [34].

We present here a significant extension of our previous work by considering different monovalent (LiCl, NaCl, KCl, and CsCl) and divalent ($CaCl_2$, $MgCl_2$, and $BaCl_2$) salt cations together with salt mixtures over a wide range of salt concentrations. Also we analyze the case of the bi-ionic potential obtained with mixtures of different salts at the same concentration. These experimental additions are not merely of an incremental nature because new insights on membrane and bi-ionic potentials are now provided under different conditions concerning the experimental technique used, the interplay between the nanostructure asymmetry and the externally imposed concentration gradient, and the different nature of the mono and divalent cations.

2. Experimental

The single-nanopore membrane is obtained from 12–μm thick polyimide (PI) foils (Kapton50 HN, DuPont) irradiated at the linear accelerator *UNILAC* (GSI, Darmstadt) with swift heavy ions (Au) of energy 11.4 MeV per nucleon. In order to achieve the desired single-ion irradiation, a metal mask incorporating a 200 micrometer-diameter centered aperture is located in front of the stack. Immediately after a single ion passes through the foil stack, it is registered by a particle detector placed behind the samples and then the ion beam is blocked. Subsequently, asymmetric track-etching techniques [36,37] are used to convert the membrane tracks into approximately conical pores. The track-etching processes produce surface pore carboxylate residues that are ionized in aqueous solution at intermediate pH values. These negatively charged groups are fixed to the pore surface and provide the cationic pore selectivity [21,22].

The SEM images of nanopore fractures and gold replicas of the conical pores, together with pore conductance measurements, give pore radii in the ranges 10–40 nm for the cone tip and 300–800 nm for the cone base [38,39]. To check the general validity of our experimental approach, different single-pore membrane samples were employed although we present only representative results obtained with two of them. For each of the pore samples, we obtain first the *I*–*V* curves at 100 and mM KCl at neutral and acidic pH values in order to verify the expected rectification and ionic selectivity characteristics. This procedure provides also relevant information on the pore characteristics [22]. For sample B, which is used in most experiments reported here, the pore base radius can be estimated from the etching time as a_{base} = 450 nm [21,22,40]. From the experimental *I*–*V* curves at acidic pH, the pore tip radius and the tip shape parameter are a_{tip} = 10 nm and d/h = 26, respectively, where d is the pore length [40]. From the experimental *I*–*V* curves at neutral pH, the surface charge density is

obtained as $\sigma = 0.9\ e/\text{nm}^2$. Additional details of this procedure can be found elsewhere [21,22,40].

Figs. 1 and 2 show the set-up used in the measurements and the experimental technique employed to determine the reversal potential, respectively. The *input* potential difference (voltage V) and the *output* current I are obtained with a couple of Ag|AgCl electrodes immersed in the two bathing solutions.

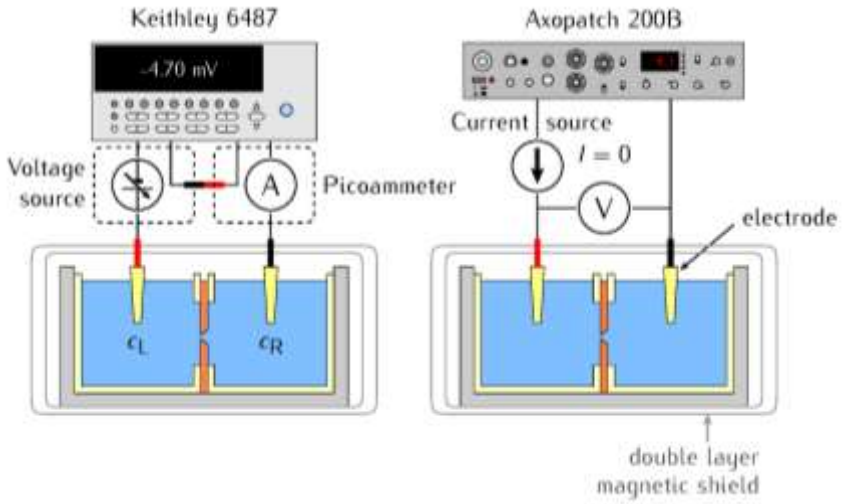

Fig. 1. Scheme of the reversal potential set-up. The single-pore membrane separates two salt solutions at different concentrations c_L and c_R under close to neutral pH values. The conical nanopore geometry and radii can be estimated from imaging the pore and from electrical conductance measurements [21,22,36,37]. Most of the reported data are obtained with a pore of radii a_{tip} = 10 nm and a_{base} = 450 nm. In the *left* set-up, the membrane potentials are obtained using a picoammeter (Keithley Instruments, Cleveland, Ohio); in the *right* set-up, an Axopatch 200B amplifier (Molecular Devices, Sunnyvale, CA) is used. In the two cases, Ag|AgCl electrodes are employed in the left (L, pore tip in the figure) and right (R, pore base in the figure) solutions together with their corresponding 2 M KCl solution salt bridges. The electrochemical cell with the single-pore is confined within a double layer magnetic shield (Amuneal Manufacturing, Philadelphia, PA) to avoid external perturbations. As a first approximation, we consider concentrations instead of activities and introduce corrections for the liquid junction potentials at the salt bridge/solution interfaces by using the Henderson equation [26,35].

The establishment and experimental characterization of steady-state membrane potentials is well-known [6-10]. In the case of nanopores, however, it is difficult to determine steady-state values of V_{mem} accurately due to the small salt fluxes involved and we have resorted here to measure V_{mem} as the reversal potential $V(I = 0)$. This alternative experimental procedure involves currents in the 10 pA range (Fig. 2a) which are close to the experimental limits of our equipment and could then be influenced by external noise. To check first the validity of the experimental approach and the consistency of the data obtained, we have undertaken preliminary measurements with a picoammeter and the Axopatch 200B (Fig. 1, *left* and *right*) amplifier using the single-pore membrane (sample A, Fig. 2). Note the good reproducibility of the membrane potentials obtained with the different set-up of Fig. 1.

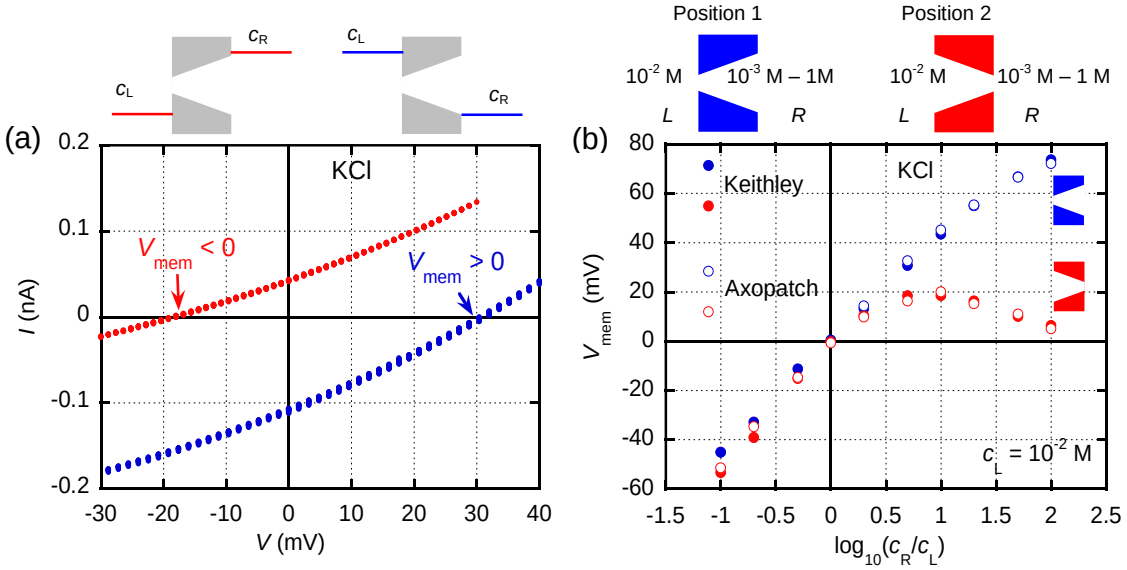

Fig. 2. (a) The membrane potential $V_{mem} = V_L - V_R$ obtained as the applied potential difference V (voltage) that gives a zero current I through the nanopore can be either positive or negative depending on the relative orientation of the conical nanopore with respect to the concentration gradient. The experimental curves correspond to KCl solutions of concentrations $c_L = 10^{-2}$ M and $c_R = 5\ 10^{-2}$ M (*left*) and $c_L = 5\ 10^{-2}$ M and $c_R = 10^{-2}$ M (*right*). (b) The corrected (full circles) and uncorrected (empty circles) values of V_{mem} as a function of $\log_{10}(c_R/c_L)$ obtained by using a picoammeter and the Axopatch 200B amplifier for membrane sample A. The size of the data points roughly corresponds to the experimental error obtained in a series of measurements. Note the significant effect of pore directionality (positions # 1 and # 2).

To allow a direct comparison, we have employed the same membrane sample B in all experiments with different chloride salt solutions of monovalent (Li^+, Na^+, K^+, and Cs^+) and divalent (Ca^{2+}, Mg^{2+}, and Ba^{2+}) cations. The membrane potentials measured should be corrected for the liquid junction potentials across the salt bridge/solution interfaces. This correction is made by using the Henderson approximation that assumes ideal solutions and a continuous solution mixture with the same functional dependence for the ionic concentration profiles [26,35].

3. Results and Discussion

Fig. 3a shows the experimental membrane potentials V_{mem} obtained for the two orientations of the asymmetric nanopore shown in the insets at the fixed KCl concentration c_L = 10^{-1} M. The line permits to quantify the deviation from the Nernstian ideal behavior observed [32]. Note also that the potential difference obtained from the *I*–*V* curves is the whole electrochemical cell potential that includes all drops across the system. The contribution of the two salt bridges at the electrodes could be significant and then both the uncorrected and liquid junction-corrected (Fig. 1) values of V_{mem} are shown for the sake of comparison. Fig. 3b considers the case c_L = 10^{-2} M, which gives higher values of V_{mem} than those of Fig. 3a when $c_R > c_L$ because of the weak Debye screening of the pore charges at low salt concentrations. Note also the significant effect of the pore directionality due to the distinct screening of the cone tip charges responsible for the selectivity to the cation. Other asymmetric systems showing directional effects are inhomogeneous and bipolar ion-exchange membranes [41-44], multifunctional cigar-shaped nanopores [23], and ion channels [45-47].

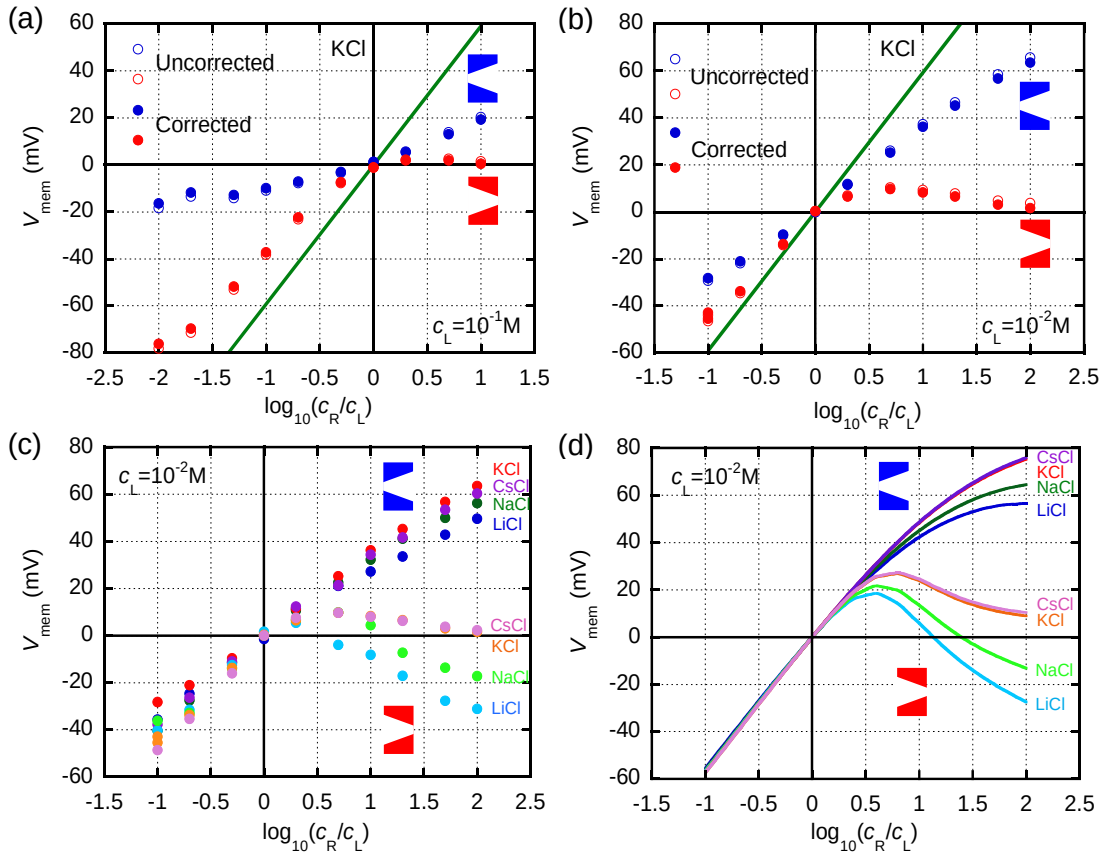

Fig. 3. (a) Uncorrected and corrected V_{mem} *vs.* $\log_{10}(c_R/c_L)$ curves for membrane sample B and the two orientations of the asymmetric nanopore shown in the insets. The KCl concentration $c_L = 10^{-1}$ M is fixed and the Nernstian line is included to better show the deviation from the ideal case. The corrected values are obtained by using the Henderson equation for the liquid junction potentials developed at the salt bridge/solution interfaces [26]. (b) V_{mem} *vs.* $\log_{10}(c_R/c_L)$ curves for $c_L = 10^{-2}$ M KCl. (c) Experimental corrected V_{mem} *vs.* $\log_{10}(c_R/c_L)$ curves for LiCl, NaCl, KCl, and CsCl solutions over a wide concentration range. (d) The corresponding theoretical curves are obtained with the Poisson-Nernst-Planck formalism described with detail in Reference [34].

To clearly show the effect of the salt concentration for the different cations, Figs. 3c and 3d consider the experimental and theoretical membrane potentials V_{mem} measured using the two orientations of the single-pore membrane. The experimental data are approximately described by the theoretical curves calculated using the Poisson-Nernst-Planck formalism with the ionic diffusion coefficients of free solutions at infinite dilution [48]. The results deviate from a straight line, especially for the case of high salt concentrations bathing the cone tip in pore position # 2. In this case, both the co- and counter-ions are allowed in the pore solution and effectively screen the surface charges [22,32,49]. Note in particular that V_{mem} tends to the small values of the liquid junction potentials characteristic of KCl and CsCl solutions.

The theoretical curves of Fig. 3d are obtained with the Poisson-Nernst-Planck formalism described with detail in Reference [34]. However, Figs. 3c and 3d suggest that the experimental limits at high and low salt concentrations could be qualitatively explained by using the Teorell-Meyer-Sievers (TMS) model; see a recent review [32] for a thorough analysis of the TMS approach and its extensions. Remarkably, all curves of Fig. 3d are obtained with the same pore charge density $\sigma = 0.9\ e/\text{nm}^2$, which gives an effective volume charge density $X = 2\sigma/(Fa_{tip}) = 0.3$ M at the pore tip for $a_{tip} = 10$ nm and the Faraday constant $F = 96500$ C/mol.

We have used ionic concentrations rather than activities in the theoretical calculations. The good agreement between experiment (Fig. 3c) and theory (Fig. 3d) has prevented us from introducing additional corrections. While this assumption should fail in the limit of high concentration, the fact is that multitude of non-ideal effects [8,29,30,50,51] may cause the external and pore solutions to deviate from the ideal behavior. Note that the charged pore appears to slightly select the less hydrated Cs^+ and K^+ cations over the more hydrated Na^+ and Li^+ cations [25].

Fig. 4a considers the counter-ion transport numbers t_+ calculated from the V_{mem} values of Fig. 3c [34]. This number constitutes a measure of the selectivity of the pore for each salt cation [25,34]. Figs. 4a and 4b show that t_+ depends not only on the external solution concentration but also on the nanostructure directionality. In particular, Fig. 4a suggests that the pore is moderately selective to cations for position # 1 all over the concentration range while Fig. 4b shows that this selectivity is lost for pore position # 2 when $c_R > c_L$, as shown by the discontinuous lines corresponding to the limiting free solution values. For position # 2 (Fig. 4b), significant cationic selectivity increments ($c_R/c_L < 1$) and reductions ($c_R/c_L > 1$) with respect to the case of position # 1 (Fig. 4a) are observed. This property could be exploited in practical applications of the conical pores [52].

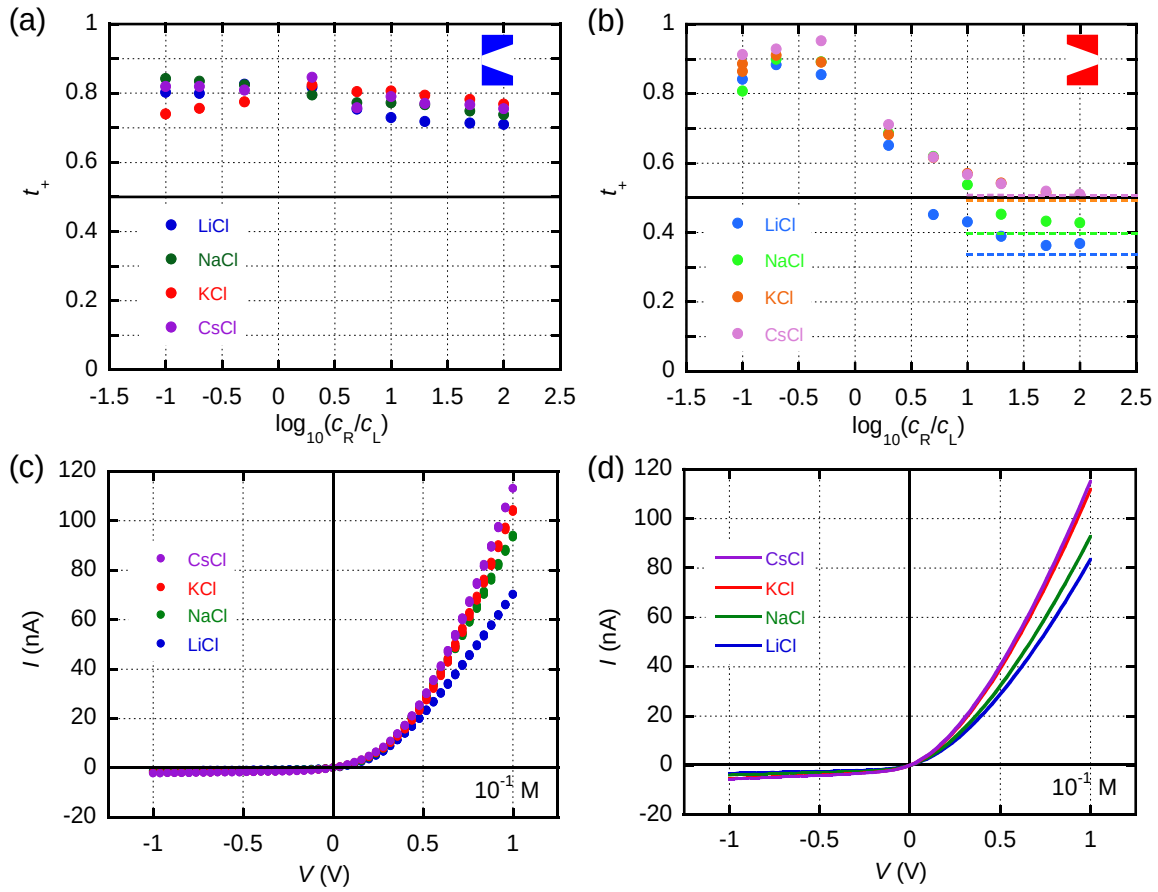

Fig. 4. (a) The cation transport numbers t_+ *vs.* $\log_{10}(c_R/c_L)$ curves for the salts of Fig. 3c and pore position # 1. (b) t_+ *vs.* $\log_{10}(c_R/c_L)$ curves for pore position # 2. The discontinuous lines correspond to the limiting free solution values. (c) The current-voltage (I–V) curves for the

monovalent salts obtained at pore position # 1 clearly show the asymmetric nanostructure characteristics [22]. The ionic conductances order observed at $V > 0$ suggests the diffusion coefficient sequence $D_{Cs} > D_K > D_{Na} > D_{Li}$ assumed in the theoretical calculations of Fig. 3d. (d) The theoretical I–V curves calculated with the cation diffusion coefficients corresponding to dilute solutions [48].

While Fig. 4a suggests that the pore selectivity is slightly different for the distinct monovalent cations, it is difficult to quantify these differences because of the pore charge screening effects and the interplay between ionic selectivity and diffusion [27]. For instance, the relative pore selectivity between two cations inferred from ionic permeability data can be different in the limits of low and high external concentrations [27]. In addition, the dependence of the membrane potentials of Fig. 3c on the nanostructure directionality makes it difficult to define a single characteristic for ionic selectivity. These questions have also been emphasized for the case of biological ion channels [27].

Figs. 4c and 4d show that the I–V curves corresponding to the asymmetric negatively charged pore have similar trends for all monovalent cations, suggesting a common conduction mechanism previously described [22,49]. The relatively high electrical resistance obtained at negative potentials gives a low current entering the cone base while the low resistance found at positive potentials gives a high current entering the cone tip [22,49]. Fig. 4c shows also that the pore is slightly sensitive to the different monovalent cations, in agreement with Fig. 3c. The experimental I–V curves give additional support to the sequence $D_{Cs} > D_K > D_{Na} > D_{Li}$ of diffusion coefficients at infinite dilution assumed in the theoretical calculations of Figs. 3d and 4d.

Figs. 5a and 5b display the uncorrected and corrected V_{mem} values for the case of a divalent cation (Ca^{2+}) at different $CaCl_2$ concentrations. The Henderson correction due to the liquid junctions at the solution/salt bridge interfaces are higher for divalent than for monovalent cations (Figs. 3a and 3b). Note also the higher Debye screening of the pore

charges by the divalent cations with respect to the case of the monovalent cations: the absolute values of V_{mem} in Figs. 5a and 5b are lower than those of Figs. 3a and 3b. Fig. 5c gives the corrected values of V_{mem} for the different divalent cations of $CaCl_2$, $MgCl_2$, and $BaCl_2$ salts and Fig. 5d shows the experimental I–V curves obtained for these divalent salts with pore position # 1. The ionic conductances follow the same sequence $D_{Ba} > D_{Ca} > D_{Mg}$ observed for these diffusion coefficients in free dilute solutions [48]. Note that the currents of Fig. 5d are much higher when the cations enter the pore tip ($V > 0$ for position # 1), in agreement with the fact that the absolute values of V_{mem} are higher when the cations diffuse from the tip to the pore base (Fig. 5c).

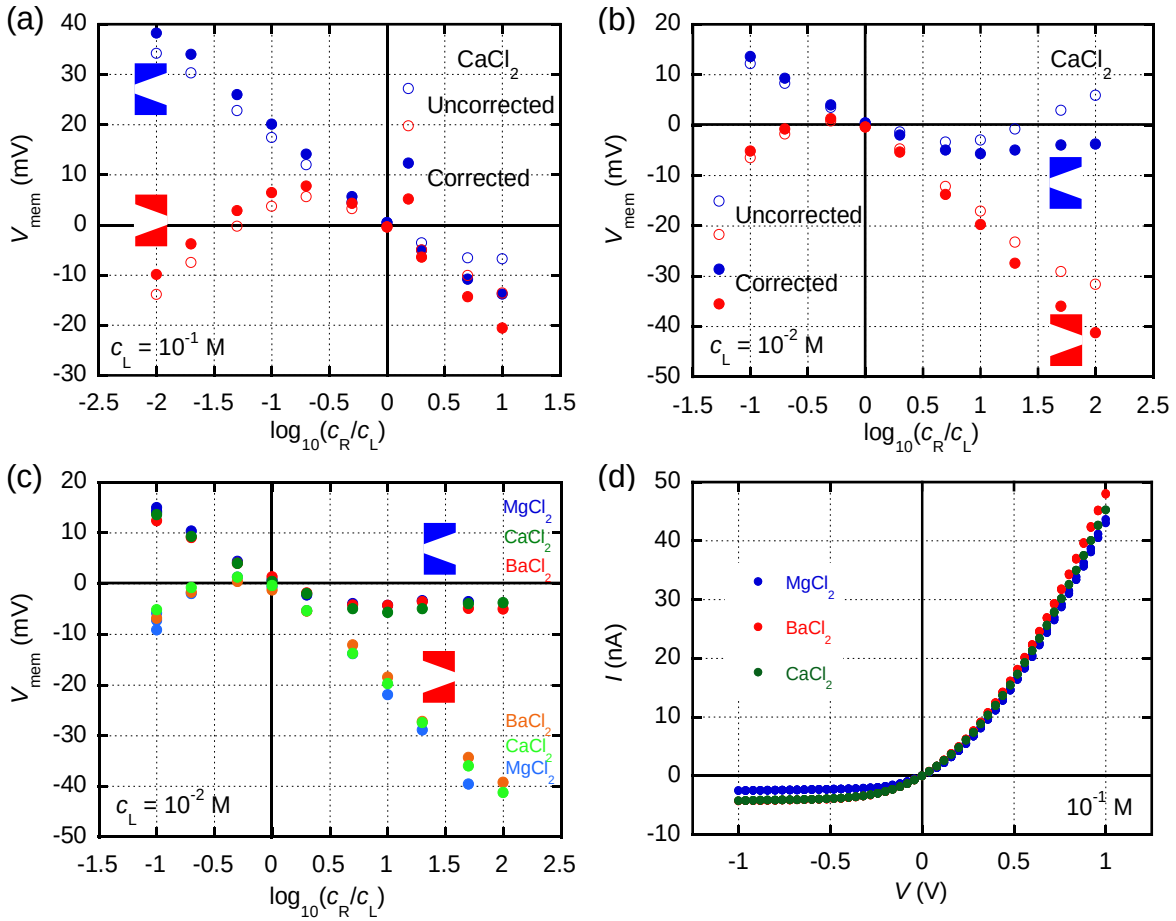

Fig. 5. (a) Uncorrected and corrected V_{mem} *vs.* $\log_{10}(c_R/c_L)$ curves for the two orientations of the asymmetric nanopore shown in the insets and the fixed $CaCl_2$ concentration $c_L = 10^{-1}$ M. (b) Experimental V_{mem} *vs.* $\log_{10}(c_R/c_L)$ curves for concentration $c_L = 10^{-2}$ M $CaCl_2$. (c) Experimental V_{mem} *vs.* $\log_{10}(c_R/c_L)$ corrected curves for $CaCl_2$, $MgCl_2$, and $BaCl_2$ salts over a

wide concentration range. (d) The *I*–*V* curves for these salts obtained at pore position # 1 give ionic conductances that show the diffusion coefficient sequence $D_{Ba} > D_{Ca} > D_{Mg}$ characteristic of free dilute solutions.

The striking similarity of all experimental V_{mem} *vs.* $\log_{10}(c_R/c_L)$ curves for the three divalent cations of Fig. 5c strongly suggests that a common electrochemical mechanism should explain the significant differences observed with respect to the case of the monovalent cations (Fig. 3c). However, previous continuum models for the membrane potential of divalent cation salts (see e.g. Refs. [53,54] and references therein) cannot reproduce the results of Fig. 5c. Note in particular the *opposite*, non-monotonic trends observed in the V_{mem} *vs.* $\log_{10}(c_R/c_L)$ curves for positions # 1 and # 2 (Figs. 5a and 5b). These opposite tendencies suggest that the relative position of the pore tip with respect to the externally imposed concentration gradient strongly influences the divalent cation concentration and electric potential gradients inside the pore.

In addition, we emphasize that the curves of Figs. 5a and 5b are almost identical for all divalent cations studied (Fig. 5c). In particular, the values of V_{mem} shown in Figs. 5a and 5b appear to follow a quasi-Nernstian straight line opposite to that of Figs. 3a and 3b only when the high salt concentration faces the pore tip for both position # 1 (*left*) and position # 2 (*right*). While this result might suggest an over-screening (charge reversal) of the pore surface charge, as observed recently for the case of solid state nanopores [55], the fact is that we did not observe any charge reversal in the experimental *I*–*V* curves of the divalent cations studied recently [56].

In absence of a quantitative description for the significant differences observed between Figs. 3c and 5c, we have attempted a qualitative explanation in Fig. 6. The cartoons attempt to emphasize the potential well due to the pore fixed charges [25,57] and the resulting ratchet potential (Fig. 6) at the conical tip [22,58]. These electrical effects are expected to be

more significant for divalent than for monovalent ions because of their different surface charge densities [25]. Also, the electrochemical mechanism invoked in Fig. 6 is general enough to apply to all divalent cations attempting to diffuse through the asymmetric nanostructure, which are characterized by similar curves in Fig. 5c.

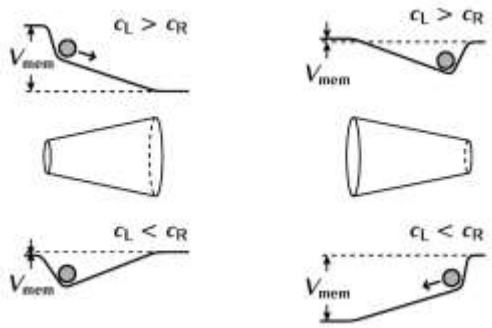

Fig. 6. The different values of $V_{mem} = V_L - V_R$ observed for pore positions # 1 (*left*) and # 2 (*right*) can be qualitatively explained in terms of the distinct relative orientations of the pore tip with respect to the divalent cation concentration gradient (Fig. 5c). The cation well due to the negative charges at the pore tip results in a non-periodic *ratchet potential* along the pore [22,58]. When the tip is bathed by the low external concentration, the electric potential distribution produces an effective trap which should be much higher for divalent than for monovalent cations. On the contrary, the shifts in the ratchet potential observed when the high external concentration bathes the pore tip help the cations to overcome the trap and give high values of V_{mem}. Note that the currents of Fig. 5d are also much higher when the cations enter the pore tip, which corresponds to $V > 0$ for position # 1.

Because of the charge-dependent rate limiting step of Fig. 6 occurring at the pore tip, the continuum theoretical model used in Fig. 3d for monovalent cations could fail in the divalent cation case. On the contrary, continuum models can still be useful for the case of the *I*–*V* curves [56] because the high voltages $V = 1$ V (see Fig. 4c and Ref. [56]) >> 0.04 V > V_{mem} (see Fig. 5c) applied in the first case allow the divalent cations to effectively surpass the potential well of Fig. 6. Note also the correspondence between the four cases considered in Fig. 6 and the experimental curves for V_{mem} of Fig. 5c that concern two opposite concentration gradients ($c_R/c_L < 1$ and $c_R/c_L > 1$) for each one of the two pore directionalities

(positions # 1 and # 2). This correspondence is not so clear at high concentration gradients because the contribution of the non-zero diffusion potentials is not included in the schematic pore ratchet potentials of Fig. 6.

To check further the different membrane potentials observed, Fig. 7a analyzes the transition from the V_{mem} values characteristic of a monovalent cation to those of a divalent cation. To this end, mixtures of KCl and $MgCl_2$ salts are considered for the two orientations of the pore. In these experiments, the external concentrations are fixed at $c_{T,L} = 10^{-1}$ M and $c_{T,R} = 10^{-2}$ M but the relative amounts of the monovalent and divalent salts contributing to the above total concentrations are varied in terms of a mixing parameter x (Fig. 7a). Remarkably, the limiting values of V_{mem} in Fig. 7a agree with those of Fig. 3a for pure KCl solutions (x = 0) and with those of Fig. 5a for pure $CaCl_2$ solutions (x = 1), which behave similarly as pure $MgCl_2$ solutions (Fig. 5c). These results confirm further the general validity of our experimental approach to the membrane potential of single conical pores.

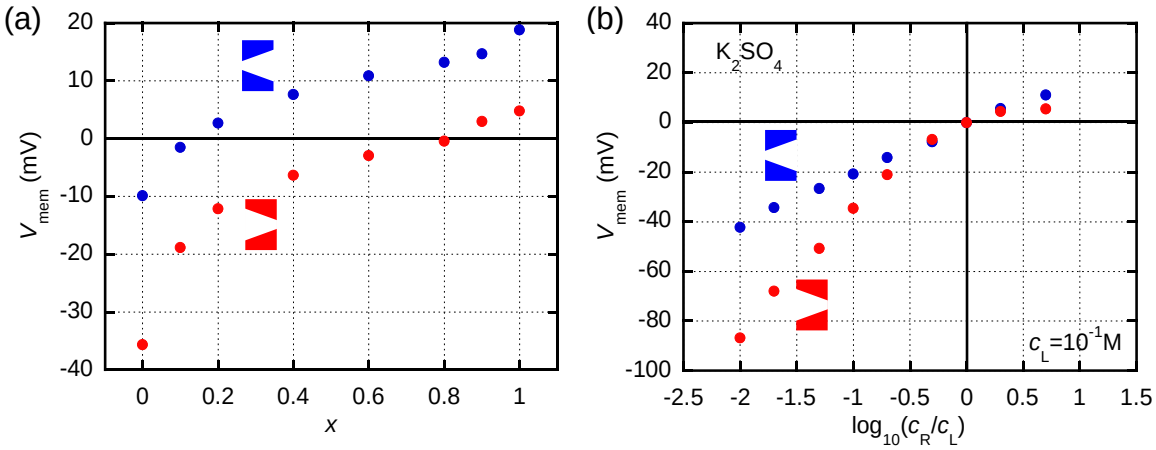

Fig. 7. (a) The experimental transition of V_{mem} between the corrected values characteristic of the monovalent (KCl) and divalent ($MgCl_2$) salts for the two pore directionalities. In this case, the total external concentrations $c_{T,L} = c_{KCl,L} + c_{MgCl_2,L} = (1–x)\ 10^{-1}$ M + $x\ 10^{-1}$ M and $c_{T,R} = c_{KCl,R} + c_{MgCl_2,R} = (1–x)\ 10^{-2}$ M + $x\ 10^{-2}$ M are kept constant but the concentrations of the monovalent and divalent salts contributing to $c_{T,L}$ and $c_{T,R}$ vary in terms of the mixing parameter x, $0 < x < 1$. (b) Experimental V_{mem} *vs.* $\log_{10}(c_R/c_L)$ corrected values for the divalent anion salt K_2SO_4 at $c_L = 10^{-1}$ M and two pore directionalities.

It should be mentioned that the two ions of Fig. 7a are crucial to cell homeostasis due to the interplay between the Mg^{2+} concentration and different Na^{+}–K^{+} pathways [59]. This is also the case of circadian rhythms in biological cells because daily magnesium fluxes regulate cellular timekeeping and energy balance [60]. The membrane potential is an instructive bioelectrical magnitude for most cellular processes [18-20,25] and is essentially regulated by the potassium concentration difference between the cell inside and the external microenvironment. As is well-known, small amounts of divalent cations in the cell inside can lead to depolarization by decreasing the absolute value of the cell $V_{mem} < 0$. Note in this context the exquisite sensitivity of the KCl-regulated V_{mem} of Fig. 7a to small additions of $MgCl_2$: the transition from $x = 0$ to $x = 0.1$ produces a large decrease in the absolute value of the observed membrane potential, suggesting a significant interplay between the monovalent and divalent cations in the regulation of V_{mem} [20,25].

Recently, the influence of divalent anions on the *I*–*V* curves and rectification phenomena of nanofluidic diodes has been considered [61]. Fig. 7b shows the V_{mem} *vs.* $\log_{10}(c_R/c_L)$ curves for K_2SO_4 solutions. In this case, it is the divalent anion SO_4^{2-} rather than the monovalent anion Cl^{-} that acts as a co-ion in the pore solution. The comparison of Fig.7b with Fig. 3a shows that the strong pore exclusion of the divalent anion (Fig. 7b) leads to absolute values of V_{mem} higher than those of the monovalent anion (Fig. 3a). Note also the significant differences obtained between the V_{mem} values of Fig. 7b (divalent co-ion) and those of Fig. 5a (divalent counter-ion).

We consider now the case of the *bi-ionic potential* V_{bip}, defined as the electrical potential difference that arises when the membrane separates two different salts which have a common ion at the same concentration. Fig. 8a shows the values of V_{bip} for three pairs of monovalent cations, with the common salt KCl. Fig. 8b considers the case of two divalent

cation salts, $CaCl_2$ in the L solution and $MgCl_2$ in the R solution. The effects due to the different directionalities of the asymmetric nanostructure are also studied.

In our theoretical approach, the bi-ionic potential is given by two interfacial Donnan potentials at the membrane/solution interfaces and the diffusion potential in the membrane phase [35,62,63]. If the two cations have similar microscopic characteristics, the Donnan potentials tend to compensate each other and then the bi-ionic potential is the membrane diffusion potential [62], which is non-zero because of the different cations in the external L and R solutions. In this way, V_{bip} depends on the salt concentration and the ionic diffusion coefficients D_{+L} and D_{+R}.

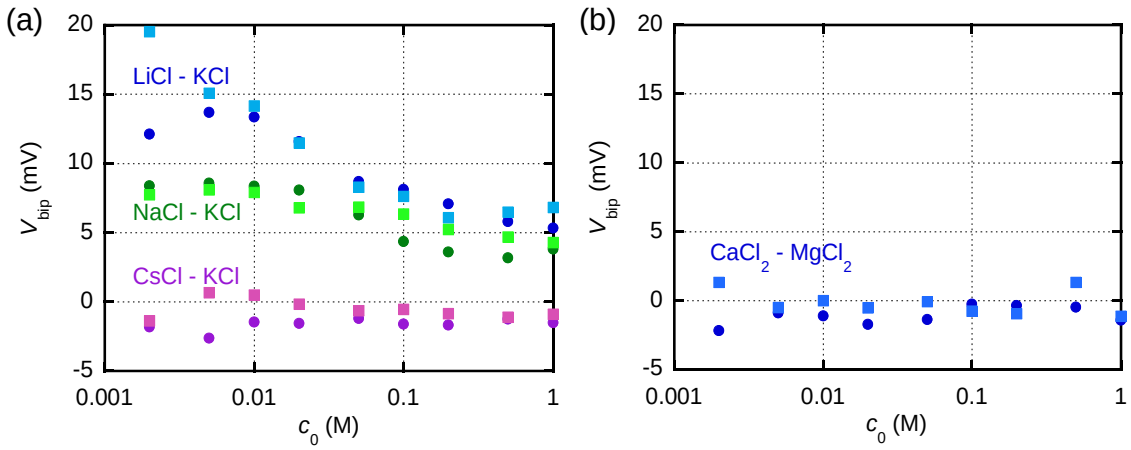

Fig. 8. (a) Corrected bi-ionic potentials V_{bip} *vs.* the external salt concentration $c_L = c_R = c_0$ for different monovalent salt configurations. The circles correspond to MCl(pore tip solution)/KCl(pore base solution) and the squares correspond to MCl(pore base solution)/KCl(pore tip solution) where M denotes the cations Li, Na, and Cs. (b) Corrected V_{bip} *vs.* c_0 for the case of two divalent cation salts. The circles correspond to the configuration $CaCl_2$(pore tip solution)/$MgCl_2$(pore base solution) and the squares to the configuration $CaCl_2$(pore base solution)/$MgCl_2$(pore tip solution).

For a symmetric membrane and a monovalent cation salt in the limit of low concentration, V_{bip} depends only on the two cation diffusion coefficients because the co-ion

(chloride) is excluded from the pore solution [22,62]. In this case, $V_{bip} = (RT/F)\ln(D_{+R}/D_{+L})$ where R is the gas constant and T the temperature [62]. The theoretical results obtained with this equation assuming dilute solution values for the ionic diffusion coefficients are 17 mV (LiCl/KCl), 10 mV (NaCl/KCl), and −1 mV (CsCl/KCl) in approximate agreement with the experimental results of Fig. 8a. In the opposite limit of high salt concentration, however, the excess of mobile ions in the pore solution effectively screen the pore charges. Thus, the chloride ion is not excluded from the pore and contributes now to V_{bip} with a diffusion coefficient D_{-}. In this case, we use the Goldman equation [35] $V_{bip} = (RT/F)\ln[(D_{+R}+D_{-})/(D_{+L}+D_{-})]$ for the liquid junction potential established between the two monovalent salts [29,62,64]. While the Goldman equation for a liquid junction is usually referred to as the "constant field equation", it is not necessary to assume a constant field to obtain it when the membrane separates two monovalent salt solutions at the same concentration [62]. Remarkably, this question was noted by Goldman himself in his original study [64]. The Goldman equation gives the theoretical values V_{bip} = 7 mV (LiCl/KCl), 4 mV (NaCl/KCl), and −0.6 mV (CsCl/KCl), in agreement with the experimental results of Fig. 8a at high salt concentration. For divalent cations, the expected values for V_{bip} should be close to zero because of the similar ionic diffusion coefficients of Ca^{2+} and Mg^{2+}, also in agreement with the results of Fig. 8b. Thus, the pore directionality effects of Fig. 5c are not so relevant in this case.

4. Conclusions

The experimental and theoretical results presented here are of fundamental interest to electrochemical membrane processes as well as to bioelectrical phenomena in cell membranes because the ions and concentration ranges considered are of technological and biological relevance. In particular, a significant conclusion emerges from the experimental data: if we

attempt to use the membrane potential as a measure of the ionic selectivity, a multitude of pore and external solution effects (nanostructure directionality and effective surface charge; cation charge number and salt concentrations) should be taken into account simultaneously. This fact has been emphasized in the case of the protein ion channels of the cell membrane [26,27]. Also, the different experimental methods to characterize the ionic selectivity of ion exchange membranes have been reviewed recently [65].

The membrane potential of conical nanopores reflects the interplay between many physico-chemical phenomena beyond the ideal (Nernstian) concentration potential. Experimental conditions such as the relative orientations of the fixed charge distribution along the pore and the external concentration gradient, the different screening of the negative pore charges by monovalent and divalent cations, and the concentrations of the different salts act together to give a wide range of non-trivial membrane potentials. Also, significant bi-ionic potentials can be obtained with mixtures of monovalent and divalent cations at the same concentration. By taking together all experimental data, we have attempted a systematic description that can contribute to the understanding of many electrochemical and bioelectrical processes regulated by the interplay between the membrane asymmetry and the ionic concentration and electrical potential gradients.

Acknowledgments

M. A., S. N., and W. E. gratefully acknowledge the financial support from the Hessen State Ministry of Higher Education, Research and the Arts (Germany), LOEWE project iNAPO. P. R., J. C., V. G., and S. M. acknowledge the funding from the *Ministerio de Economia y Competitividad* and the European Regional Development Funds (FEDER), project MAT2015-65011-P. The authors acknowledge Prof. J. A. Manzanares for fruitful discussions.

References

[1] B. Sales, M. Saakes, J.W. Post, C. J. N. Buisman, P. M. Biesheuvel, H. V. M. Hamelers, Direct power production from a water salinity difference in a membrane-modified supercapacitor flow cell, Environ. Sci. Technol. 44 (2010) 5661–5665.

[2] R. Li, J. Jiang, Q. Liu, Z. Xie, J. Zhai, Hybrid nanochannel membrane based on polymer/MOF for high performance salinity gradient power generation, Nano Energy 53 (2018) 643–649.

[3] P. Długołęcki, K. Nymeijer, S. Metz, M. Wessling, Current status of ion exchange membranes for power generation from salinity gradients, J. Membrane Sci, 319 (2008) 214–222.

[4] W. Guo, L. Cao, J. Xia, F.-Q. Nie, W. Ma, J. Xue, Y. Song, D. Zhu, Y. Wang, L. Jiang, Energy harvesting with single-ion-selective nanopores: A concentration-gradient-driven nanofluidic power source, Adv. Funct. Mater. 20 (2010) 1339–1344,

[5] L.-J. Cheng, Electrokinetic ion transport in nanofluidics and membranes with applications in bioanalysis and beyond, Biomicrofluidics 12 (2018) 021502.

[6] D. R. Díaz, F. J. Carmon, L. Palacio, N. A. Ochoa, A. Hernández, P. Pradanos, Impedance spectroscopy and membrane potential analysis of microfiltration membranes. The influence of surface fractality, Chem. Eng. Sci. 178 (2018) 27–38.

[7] J. Benavente, A study of membrane potential across a cellophane membrane for different electrolytes, J. Non-Equilib. Thermodyn. 9 (1984) 217–224.

[8] T. S. Sorensen, J. B. Jensen, Membrane charge and donnan distribution of ions by electromotive force (EMF) measurements on a homogeneous cellulose acetate membrane, J. Non-Equilib. Thermodyn. 9 (1984) 1–34.

[9] T. S. Sorensen, J. B. Jensen, B. Malmgren-Hansen, Electromotive force and impedance studies of cellulose acetate membranes: Evidence for two binding sites for divalent cations and for an alveolar structure of the skin layer, Desalination, 80 (1991) 265–299.

[10] V. M. Barragán, C. Ruíz-Bauzá, Membrane potentials and electrolyte permeation in a cation- exchange membrane, J Membrane Sci., 154 (1999) 261–272.

[11] K. R. Ward, E. J. F. Dickinson, R. G. Compton, Dynamic theory of membrane potentials, J. Phys. Chem. B 114 (2010) 10763–10773.

[12] D. Momotenko, F. Cortes-Salazar, J. Josserand, S. Liu, Y. Shaob, H. H. Girault, Ion current rectification and rectification inversion in conical nanopores: a perm-selective view, Phys. Chem. Chem. Phys. 13 (2011) 5430–5440.

[13] L-H. Yeh, C. Hughes, Z. Zeng, S. Qian, Tuning ion transport and selectivity by a salt gradient in a charged nanopore, Anal. Chem. 86 (2014) 2681 − 2686.

[14] J. P. Hsu, S. C. Lin, C. Y. Lin, S. Tseng, Power generation by a pH-regulated conical nanopore through reverse electrodialysis, J. Power Sources 366 (2017) 169–177.

[15] B. Balannec, A. Ghoufi, A. Szymczyk, Nanofiltration performance of conical and hourglass nanopores, J. Membrane Sci. 552 (2018) 336–340.

[16] S. Balme, T. Ma, E. Balanzat, J. M. Janot, Large osmotic energy harvesting from functionalized conical nanopore suitable for membrane applications, J. Power Sources 544 (2017) 18–24.

[17] M. Lepoitevin, T. Ma, M. Bechelany, J. M. Janot, S. Balme, Functionalization of single solid state nanopores to mimic biological ion channels: A review, Adv. Colloid Interface Sci. 250 (2017) 195–213.

[18] M. Levin, Reprogramming cells and tissue patterning via bioelectrical pathways: molecular mechanisms and biomedical opportunities. Wiley Interdiscip. Rev.-Syst. Biol. Med. *5* (2013) 657–676.

[19] J. Cervera, A. Pietak, M. Levin, S. Mafe, Bioelectrical coupling in multicellular domains regulated by gap junctions: a conceptual approach. Bioelectrochem. 123 (2018) 45–61.

[20] M. Yang, W. J. Brackenbury, Membrane potential and cancer progression, Front Physiol, 4 (2013) 185.

[21] Z. Siwy, I. D. Kosinska, A. Fulinski, C. R Martin, Asymmetric Diffusion through Synthetic Nanopores, Phys. Rev. Lett. 94 (2005) 048102.

[22] J. Cervera, B. Schiedt, R. Neumann, S. Mafe, P. Ramirez, Ionic conduction, rectification, and selectivity in single conical nanopores, J. Chem. Phys. 124 (2006) 104706.

[23] P. Ramirez, M. Ali, W. Ensinger, S. Mafe, Information processing with a single multifunctional nanofluidic diode, Appl. Phys. Lett. 101 (2012) 133108.

[24] M. Queralt-Martín, E. Garcia-Gimenez, V. M. Aguilella, P. Ramírez, S. Mafé, A. Alcaraz Electrical pumping of potassium ions against an external concentration gradient in a biological ion channel, Appl. Phys. Lett. 103 (2013) 043707.

[25] B. Hille, Ion channels of excitable membranes, Sinauer Associates, Sunderland, 1992.

[26] A. Alcaraz, E. M. Nestorovich, M. Lidon Lopez, E. Garcıa-Gimenez, S. M. Bezrukov, V. M. Aguilella, Diffusion, exclusion, and specific binding in a large channel: A study of OmpF selectivity inversion, Biophys. J. 96 (2009) 56–66.

[27] M. L. Lopez, E. Garcia-Gimenez, V. M. Aguilella, A. Alcaraz, Critical assessment of OmpF channel selectivity: merging information from different experimental protocols, J. Phys.: Condens. Matter. 22 (2010) 454106.

[28] J. Cervera, S. Meseguer, S. Mafe, The interplay between genetic and bioelectrical signaling permits a spatial regionalization of membrane potentials in model multicellular ensembles, Sci. Rep. 6 (2016) 35201.

[29] N. Lakshminarayanaiah, Equations of membrane biophysics, Academic Press: New York, 1984.

[30] F. G. Helfferich, Ion exchange, McGraw-Hill, New York, 1962.

[31] H. Strathmann, Ion-exchange membrane separation processes, Elsevier, Amsterdam, 2004.

[32] A. H. Galama, J. W. Post, H. V. M. Hamelers, V. V. Nikonenko, P. M. Biesheuvel, On the origin of the membrane potential arising across densely charged ion exchange membranes: How well does the Teorell-Meyer-Sievers theory work?, J. Membrane Sci. Res. 2 (2016) 128–140.

[33] D. J. Blackiston, K. A. McLaughlin, M. Levin, Bioelectric controls of cell proliferation: Ion channels, membrane voltage and the cell cycle, Cell Cycle 8 (2009) 83527–3536.

[34] J. Cervera, A. Alcaraz, B. Schiedt, R. Neumann, P. Ramirez, Asymmetric selectivity of synthetic conical nanopores probed by reversal potential measurements, J. Phys. Chem. C 111 (2007) 12265–12273.

[35] K. Kontturi, L. Murtomäki, J. A. Manzanares, Ionic transport processes: in Electrochemistry and Membrane Science, Oxford University Press, New York, 2008.

[36] Z. Siwy, D. Dobrev, R. Neumann, C. Trautmann, K. Voss, Electro-responsive asymmetric nanopores in polyimide with stable ion-current signal, Appl. Phys. A 76 (2003) 781–785.

[37] P. Apel, Track etching technique in membrane technology, Radiat. Meas. 34 (2001) 559–566.

[38] M. Ali, P. Ramirez, S. Mafe, R. Neumann, W. Ensinger, A pH-tunable nanofluidic diode with a broad range of rectifying properties, ACS Nano 3 (2009) 603–608.

[39] P. Ramirez, V. Garcia-Morales, V. Gomez, M. Ali, S. Nasir, W. Ensinger, S. Mafe, Hybrid circuits with nanofluidic diodes and load capacitors, Phys. Rev. Applied 7 (2017) 064035.

[40] P. Ramirez, P. Y. Apel, J. Cervera, S. Mafe, Pore structure and function of synthetic nanopores with fixed charges: Tip shape and rectification properties, Nanotechnology 19 (2008) 315707.

[41] J. A. Manzanares, S. Mafe, J. Pellicer, Transport phenomena and asymmetry effects in membranes with asymmetric fixed charge-distributions, J. Phys. Chem. 95 (1991) 5620–5624.

[42] A. V. Sokirko, P. Ramirez, J.A. Manzanares, S. Mafé, Modelling of forward and reverse bias conditions in bipolar membranes. Ber. Bunsenges Phys. Chem. 97 (1993) 1040–1049.

[43] P. Ramirez, S. Mafé, J.A. Manzanares, J. Pellicer, Membrane potential of bipolar membranes, J. Electroanal. Chem. 404 (1996) 187–193.

[44] A. Alcaraz, P. Ramirez, S. Mafe, H. Holdik, B. Bauer, Ion selectivity and water dissociation in polymer bipolar membranes studied by membrane potential and current–voltage measurements, Polymer 41 (2000) 6627–6634.

[45] Cervera, A. G. Komarov, V. M. Aguilella, Rectification properties and pH-dependent selectivity of meningococcal class 1 porin, Biophys. J. 94 (2008) 1194–1202.

[46] E. García-Giménez, A. Alcaraz, V. M. Aguilella, P. Ramirez, Directional ion selectivity in a biological nanopore with bipolar structure, J. Membrane Sci. 331 (2009) 137–142.

[47] C. Verdia-Baguena, V. Gomez, J. Cervera, P. Ramirez, S. Mafe, Energy transduction and signal averaging of fluctuating electric fields by a single protein ion channel, Phys. Chem. Chem. Phys. 19 (2017) 292–296.

[48] R. A. Robinson, R. H. Stokes, Electrolyte Solutions, Butterworth Scientific Publications, London, 1955.

[49] T. Gamble, K. Decker, T. S. Plett, M. Pevarnik, J.-F. Pietschmann, I. Vlassiouk, A. Aksimentiev, Z. S. Siwy, Rectification of ion current in nanopores depends on the type of monovalent cations: Experiments and modeling, J. Phys. Chem. C 118 (2014) 9809−9819.

[50] S. Mafé, P. Ramírez, A. Tanioka, J. Pellicer, Model for counterion-membrane-fixed ion pairing and Donnan equilibrium in charged membranes, J. Phys. Chem. B 101 (1997) 1851–1856.

[51] S. Mafé, P. Ramírez, J. Pellicer, Activity coefficients and Donnan coion exclusion in charged membranes with weak-acid fixed charge groups, J. Membrane Sci. 138 (1998) 269–277.

[52] J. Cervera, P. Ramirez, S. Mafe, P. Stroeve, Asymmetric nanopore rectification for ion pumping, electrical power generation, and information processing applications, Electrochim. Acta 56 (2011) 4504–4511.

[53] Y. Lanteri, A. Szymczyk, P. Fievet. Membrane potential in multi-ionic mixtures, J. Phys. Chem. B 113 (2009) 9197–9204.

[54] W.-J. Shang, X.-L. Wang, Y.-X. Yu, Theoretical calculation on the membrane potential of charged porous membranes in 1-1, 1-2, 2-1 and 2-2 electrolyte solutions, J. Membrane Sci. 285 (2006) 362–375.

[55] S. X. Li, W. Guan, B. Weiner, M. A. Reed, Direct observation of charge inversion in divalent nanofluidic devices, Nanolett. 15 (2015) 5046−5051.

[56] P. Ramirez, J. A. Manzanares, J. Cervera, V. Gomez, M. Ali, I. Pause, W. Ensinger, S. Mafe, Nanopore charge inversion and current-voltage curves in mixtures of asymmetric electrolytes, J. Membrane Sci. 563 (2018) 633–642.

[57] S. Mafe, J. A. Manzanares, P. Ramirez, Modeling of surface vs. bulk ionic conductivity in fixed charge membranes, Phys. Chem. Chem. Phys. 5 (2003) 376–383.

[58] Z. Siwy, A. Fulinski, Fabrication of a Synthetic Nanopore Ion, Phys. Rev. Lett. 89 (2002) 198103.

[59] M. Bara, A. Guiet-Bara, J. Durlach, Regulation of sodium and potassium pathways by magnesium in cell membranes, Magnes. Res. 6 (1993) 167–177.

[60] K. A. Feeney, L. L. Hansen, M. Putker, C. Olivares-Yañez, J. Day, L. J. Eades, L. F. Larrondo, N. P. Hoyle, J. S. O'Neill, G. van Ooijen, Daily magnesium fluxes regulate cellular timekeeping and energy balance, Nature 532 (2016) 375.

[61] G. Perez-Mitta, A. G. Albesa, M. E. T. Molares, C. Trautmann, O. Azzaroni, The influence of divalent anions on the rectification properties of nanofluidic diodes: Insights from experiments and theoretical simulations, ChemPhysChem 17 (2016) 2718–2725.

[62] A. Guirao, S. Mafé, J. A. Manzanares, J. A. Ibáñez, Biionic potential of charged membranes: Effects of the diffusion boundary layers, J. Phys. Chem. 99 (1995) 3387–3393.

[63] L. Dammak, C. Larchet, B. Auclair, J.A. Manzanares, S. Mafe, The influence of the salt concentration and the diffusion boundary layers on the bi-ionic potential, J. Membrane Sci. 119 (1996) 81–90.

[64] D. E. Goldman, Potential, impedance, and rectification in membranes, J Gen. Physiol. 27 (1943) 37–60.

[65] T. Luo, S. Abdu, M. Wessling, Selectivity of ion exchange membranes: A review, J. Membrane Sci. 555 (2018) 429–454.

TOC image

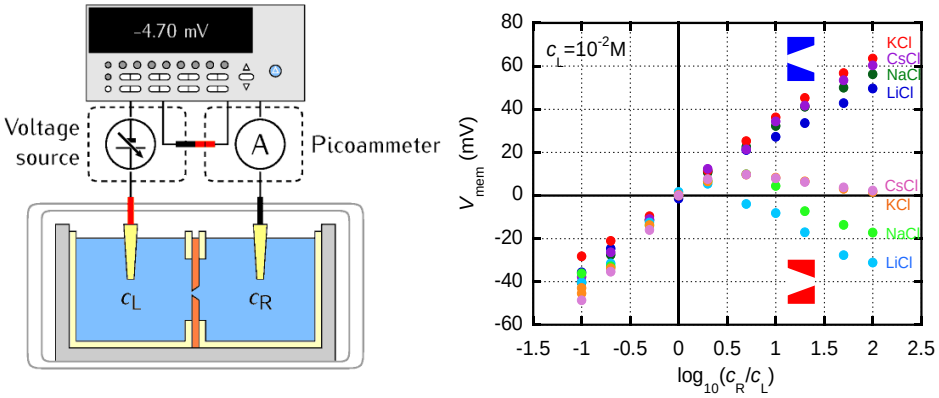
-4.70 mV
Voltage source
A
Picoammeter
c_L
c_R
c_L =10^{-2}M
KCl
CsCl
NaCl
LiCl
CsCl
KCl
NaCl
LiCl
V_{mem} (mV)
$\log_{10}(c_R/c_L)$